

Topological Defects and Defects-free states in toroidal nematics

Han Miao

Department of Physics, Shanghai Jiao Tong University, Shanghai 200240 China

Yao Li

*Department of Physics, Tsinghua University, Beijing 100084, China and
Department of Physics, Shanghai Jiao Tong University, Shanghai 200240 China*

Hongru Ma*

*The State Key Laboratory Of Metal Matrix Composites
Key Laboratory of Artificial Structures and Quantum Control (Ministry of Education) and
School of Mechanical Engineering, Shanghai Jiao Tong University, Shanghai 200240 China*

(Dated:)

Abstract

We investigated the nematic ordering on a torus by means of analytic method and the method of simulated annealing, the Frank free energy, both in the standard form and covariant form, were used in the study. The defect free state was found to be the ground state in both cases. However, in the case of the standard model, there are two kinds of defective free ordering and a transition between the two occurs at a critical value of radius ratio $k = \frac{r}{R}$. The first one is $\theta = 0$ in the small k regime and the second one is a variable θ with position of the torus. In the case of the covariant model the ground state is confirmed to be the infinitely degenerate of θ equals to a random constant. The states with defects are the excited states, where the pairs of defects excited and, duo to the barrier between positive and negative defects, have pretty long life. The behavior of the defect state basically the same for both of the two models.

* hrma@sjtu.edu.cn

I. INTRODUCTION

Interplays of order and geometry play fundamental roles in many physical systems[? ?]. In-plane order on a two-dimensional curved surface attracted research interests in recent years since the discoveries of ordered phases L_β and P_β in phospholipid membranes[?]. After the pioneer work by Nelson and Peliti[?] on interplay of crystalline and hexatic order on fluctuating membranes, quite a lot of researches are done for understanding the relation between in-plane order and the geometry where it live on.

Lubensky and Prost [?] showed that the equilibrium positions of topological defects for smectic-C order on a spherical vesicle are on two opposite poles of the sphere, while the topological defects of the nematic order and hexatic order on a spherical vesicle stay at the corner of a tetrahedron and an icosahedron, respectively, and Park, Lubensky and MacKintosh[?] extended this study to deformable spherical vesicles. Nelson[?] proposed a possible application of these defects as attachment points for chemical linkers, suitable for molecular self-assembly. One example of this promising route of designing superstructure materials has been achieved for divalent case by Smectic-C tilt order [?]. In recent years, a number of experimental, theoretical and simulation studies have been dedicated to the issue of nematic and hexatic order on spherical surfaces [? ? ? ? ? ?].

Besides the intensive studies of spherical topology surfaces, vesicles of toroidal topology gave rise to interest after prediction and first experiment observation of toroidal vesicles[? ?] more than 20 years ago. Evans first gave a theoretical discussion on covariant model of p -atic order on a toroidal membrane[?], revealing topological defects may appear in ground state even not required by topological constraints. Then Bowick, Nelson and Travesset investigated hexatic order in toroidal geometries more extensively[?]. And 3D derivative XY Model on toroidal surface was studied by Seilinger et. al.[?] using Monte Carlo methods very recently.

In this paper, we describe nematic order on toroidal surface by studies of two different models, covariant derivative and 3D derivative Franck free energy models, depending on the molecular details of a real system, both of the two models can be approximate models for real systems. These models can be used to describe toroidal vesicles self-assembly by amphiphilic liquid crystalline side-chain block copolymers, where experimental examples of the spherical topology were achieved by Jia et. al.[? ?]. By using both numerical and Monte Carlo

methods, we investigate these two models, exploring the defect-free and defective structures for toroidal surfaces at various parameters extensively.

II. MODEL AND METHODS

The purpose of this study is to investigate the nematic orders on the torus, thus we first define our problem and give the method of study in detail. The torus to be studied is a circular torus with radius R , the distance between the center of the torus and the center of the tube, and with tube radius r . In fact, here only the ratio R/r is an independent variable, however, we keep the two for clarity of the following presentation. The coordinate system is chosen in the following, the z axis is perpendicular to the plane of the large circle of the torus, and xy plane is the plane of the circle, the origin of the coordinate system is taken to be the center of the torus. In this system of coordinates, a point on the torus can be specified by two parameters α and β , both varies from 0 to 2π , represent the angle of the projection to xy plane of the position vector with respect to x axis and the local angle of the point with respect to the xy plane when taking the intersection of the projection and the center circle of the tube as the origin. A sketch of the coordinate system is shown in Fig.1. With the two parameters α and β , the coordinates of a point on the torus is given by

$$\mathbf{X} = \begin{pmatrix} \cos \alpha (R + r \cos \beta) \\ \sin \alpha (R + r \cos \beta) \\ r \sin \beta \end{pmatrix} \quad (1)$$

The in-plane nematic liquid crystal order is modeled by a director field $\hat{n}(\mathbf{x})$, which is a unit headless director field living in the tangent plane of the toroidal surface. Similar to a previous study for tilt order on curved surface by J. V. Selinger et al Ref.?, the nematic elastic energy is taken to be the standard Frank free energy form

$$F = \int K (\nabla \hat{n})^2 dA \quad (2)$$

where $\nabla \hat{n}$ is the three-dimensional (3D) gradient of headless director field \hat{n} . For comparison, we also consider the covariant gradient Frank free energy model[?]]

$$F = \int K (D\hat{n})^2 dA \quad (3)$$

where $D\hat{n}$ denotes the covariant gradient of \hat{n} .

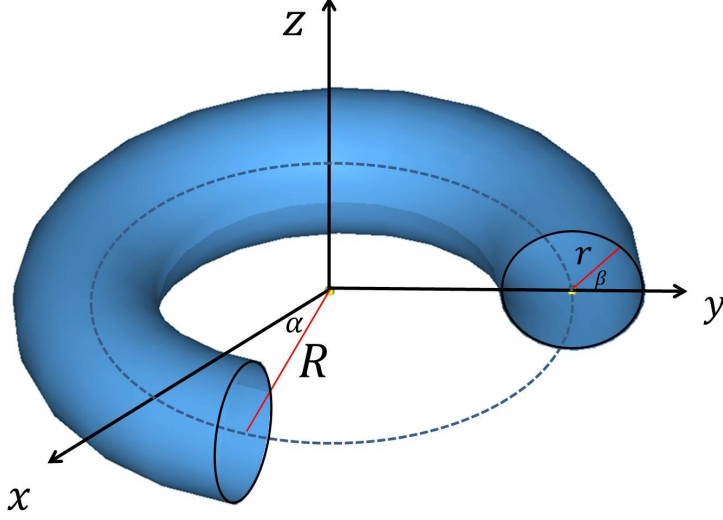


Figure 1. The coordinate system and parametrization of a circular torus of radii R and r .

The discretization is necessary in order to do numerical simulations, in this calculation the toroidal surface is discretized into a triangular lattice. For each triangle i , we assign an in-plane unit vector \hat{n}_i to represent its local in-plane liquid crystal order. The unit vector pairs \hat{n}_i and \hat{n}_j interact with each other only when the triangles i and j are nearest neighbors. For the 3D gradient model, the Frank free energy on the discretized surface is given by the following expression

$$F = 2K \sum_{\langle ij \rangle} S_{ij} d_{ij}^{-2} \{1 - [\hat{n}_i \cdot \hat{n}_j]^2\}. \quad (4)$$

Here d_{ij} is the bond length connecting v_i and v_j where v_i denotes the center of the triangle i . $S_{ij} = S_{\Delta v_i ab} + S_{\Delta v_j ab}$, where $S_{\Delta v_i ab}$ and $S_{\Delta v_j ab}$ are the areas of the two triangles with vertices (v_i, a, b) and (v_j, a, b) respectively, a and b are the two end points of the edge shared by triangles i and j . When the area S_{ij} tends to zero the discretized form approaches to the correct continuum limit 2 as expected.

For the covariant gradient model Eq.3, the discrete free energy form is given by

$$F = 2K \sum_{\langle ij \rangle} S_{ij} d_{ij}^{-2} \{1 - [\hat{n}_i \cdot \Gamma(j, i) \hat{n}_j]^2\} \quad (5)$$

where $\Gamma(j, i) \hat{n}_j$ is the parallel transport operation that transports the vector \hat{n}_j from triangle

j to i , given by[?]

$$\Gamma(j, i) \hat{n}_j = (\hat{n}_j \cdot \hat{\zeta}_{ji}) \hat{\zeta}_{ij} + [\hat{n}_j \cdot (\hat{e}_j \times \hat{\zeta}_{ji})] (\hat{e}_i \times \hat{\zeta}_{ij}) \quad (6)$$

where $\zeta_{ij} = \mathbf{P}_i \hat{r}_{ij}$ is the best estimate for the directions of geodesic connecting the center of triangle i and j , here \hat{r}_{ij} is the direction vector connecting them and \mathbf{P}_i is the plane projector of triangle i .

Now we describe our simulation method. The ordering configuration is determined by the minimization of the free energy numerically in the discrete form, however, direct minimization is impractical because the number of variables is very large. Thus the simulated annealing Monte Carlo method is employed for the minimization of the free energy. The initial configuration is the randomly assigned nematic vectors to each triangles, then the nematic vector of a random picked triangle is randomly rotated within the tangent plane. The acceptance probability for each move is given by the Metropolis rule

$$P_{acc} = \min \{1, \exp(-\Delta F/k_b T)\} \quad (7)$$

where ΔF is the free energy difference before and after a move. The initial temperature is high enough and then lowered in every 5000 Monte Carlo steps. When the temperature is low enough so that a definite configuration emerges, the calculation stopped.

III. RESULTS AND DISCUSSION

A. Defect-free states

According to Poincaré-Hopf theorem, the sum of the winding numbers of all in-plane order defects equals to the Euler characteristic number χ of the topological surface they live in. Particularly for toroidal surface, with Euler characteristic number $\chi = 0$, the net winding number of all topological defects should be zero.

First we consider the defect-free states for 3D gradient model described by equation 2.

The two perpendicular tangent vectors of the toroidal surface are given by

$$\begin{aligned}\mathbf{X}_\alpha &= \begin{pmatrix} -\sin \alpha (R + r \cos \beta) \\ \cos \alpha (R + r \cos \beta) \\ 0 \end{pmatrix} \\ \mathbf{X}_\beta &= \begin{pmatrix} -r \cos \alpha \sin \beta \\ -r \sin \alpha \sin \beta \\ r \cos \beta \end{pmatrix}\end{aligned}\tag{8}$$

and the covariant form of the metric tensor is evaluated from the tangent vectors as:

$$g_{ij} = \begin{pmatrix} \mathbf{X}_\alpha \cdot \mathbf{X}_\alpha & \mathbf{X}_\alpha \cdot \mathbf{X}_\beta \\ \mathbf{X}_\alpha \cdot \mathbf{X}_\beta & \mathbf{X}_\beta \cdot \mathbf{X}_\beta \end{pmatrix} = \begin{pmatrix} (R + r \cos \beta)^2 & 0 \\ 0 & r^2 \end{pmatrix}\tag{9}$$

with is corresponding contravariant form

$$g^{ij} = \begin{pmatrix} \frac{1}{(R+r \cos \beta)^2} & 0 \\ 0 & \frac{1}{r^2} \end{pmatrix}\tag{10}$$

$$\sqrt{g} = \det(g_{ij}) = r (R + r \cos \beta)\tag{11}$$

The nematic vector can be represented by its orientation angle θ in the tangent space by

$$\hat{\mathbf{n}} = \cos \theta \hat{\mathbf{X}}_\alpha + \sin \theta \hat{\mathbf{X}}_\beta\tag{12}$$

where the orientation angle is a function of the parameters α and β , $\theta = \theta(\alpha, \beta)$, and the normalized tangent vectors are

$$\begin{aligned}\hat{\mathbf{X}}_\alpha &= \begin{pmatrix} -\sin \alpha \\ \cos \alpha \\ 0 \end{pmatrix} \\ \hat{\mathbf{X}}_\beta &= \begin{pmatrix} -\cos \alpha \sin \beta \\ -\sin \alpha \sin \beta \\ \cos \beta \end{pmatrix}\end{aligned}\tag{13}$$

The free energy (2) can be explicitly parametrized in this representation as

$$F/K = \oint_{torus} (\nabla \hat{\mathbf{n}})^2 dS = \int \int \sqrt{g} \sum_{i,j=\alpha,\beta} g^{ij} \partial_i \hat{\mathbf{n}} \cdot \partial_j \hat{\mathbf{n}} d\alpha d\beta\tag{14}$$

The derivatives of the nematic vectors are

$$\begin{aligned}\partial_\alpha \hat{\mathbf{n}} &= \cos \theta \hat{\mathbf{X}}_{\alpha\alpha} - \sin \theta \theta_\alpha \hat{\mathbf{X}}_\alpha + \sin \theta \hat{\mathbf{X}}_{\beta\alpha} + \cos \theta \theta_\alpha \hat{\mathbf{X}}_\beta \\ \partial_\beta \hat{\mathbf{n}} &= \cos \theta \hat{\mathbf{X}}_{\alpha\beta} - \sin \theta \theta_\beta \hat{\mathbf{X}}_\alpha + \sin \theta \hat{\mathbf{X}}_{\beta\beta} + \cos \theta \theta_\beta \hat{\mathbf{X}}_\beta\end{aligned}\tag{15}$$

In the above expression the subscript means the partial differentiation with respect to the variable. The derivatives of the unit tangent vectors are given by

$$\begin{aligned}\hat{\mathbf{X}}_{\alpha\alpha} &= \begin{pmatrix} -\cos \alpha \\ -\sin \alpha \\ 0 \end{pmatrix} \\ \hat{\mathbf{X}}_{\alpha\beta} &= \begin{pmatrix} 0 \\ 0 \\ 0 \end{pmatrix} \\ \hat{\mathbf{X}}_{\beta\alpha} &= \begin{pmatrix} \sin \alpha \sin \beta \\ -\cos \alpha \sin \beta \\ 0 \end{pmatrix} \\ \hat{\mathbf{X}}_{\beta\beta} &= \begin{pmatrix} -\cos \alpha \cos \beta \\ -\sin \alpha \cos \beta \\ -\sin \beta \end{pmatrix}\end{aligned}\tag{16}$$

It is clear that the torus is symmetric with the rotation about z axis, if we assume that the nematic order has the same symmetry, then the θ will be function of β only. We consider this simple case first in the following. By substituting Eq.(10), Eq.(11), Eq.(15) and Eq.(16) into the free energy functional (26) and considering that $\theta_\alpha = 0$ from symmetry assumption mentioned above, the free energy is derived as

$$\begin{aligned}F[\theta]/K &= \int \int d\alpha d\beta r (R + r \cos \beta) \\ &\quad \cdot \left[\frac{\left(\frac{1}{4} (3 - \cos 2\beta + 2\cos^2 \beta \cos 2\theta) + 2\sin \beta \theta_\alpha + \theta_\alpha^2 \right)}{(R + r \cos \beta)^2} + \frac{\sin^2 \theta + \theta_\beta^2}{r^2} \right] \\ &= \int \int d\alpha d\beta \frac{R + r \cos \beta}{r} \cdot \left[\theta_\beta^2 + \sin^2 \theta + \frac{r^2 \cos^2 \beta}{2(R + r \cos \beta)^2} \cos 2\theta \right] + const \\ &= \int \int d\alpha d\beta \frac{R + r \cos \beta}{r} \cdot \left[\theta_\beta^2 + \left(1 - \frac{r^2 \cos^2 \beta}{(R + r \cos \beta)^2} \right) \sin^2 \theta \right] + const\end{aligned}\tag{17}$$

Denote the ratio of the two radii as k , $k \equiv r/R$, and the coefficient of $\sin^2 \theta$ as $q(\beta) \equiv 1 - \frac{r^2}{(R + r \cos \beta)^2} \cos^2 \beta$. It is obvious that the minimum of $q(\beta)$ is $q(\pi) = 1 - \frac{1}{(k^{-1} - 1)^2}$ at $\beta = \pi$,

and this minimum value is positive when $k < \frac{1}{2}$. Thus, $q(\beta) > 0$ for all β when $k < \frac{1}{2}$ and the free energy is a minimum when $\theta \equiv 0$. As we will discuss shortly, this minimum is in fact the ground state of the system. When $k > \frac{1}{2}$, $q(\pi) < 0$, then $\theta = 0$ can not be the minimum free energy configuration. On the outer circle, where $\beta = 0$ and $q(0) > 0$, $\theta = 0$ is the most favorable configuration, i.e., the nematic vector goes around the symmetry axis. In the inner circle, for a very fat torus that the ratio k closes to 1, The coefficient of $\sin^2 \theta$ is negative in the region so that $\sin^2 \theta$ takes its maximum value in order to minimize the local free energy density, thus favors $\theta = \pi/2$, i.e. vector parallels to the symmetry axis. From these observation it is clear that a constant θ could not minimize the total free energy. In order to find the solution of θ for these cases, we follow the standard procedure to find the result. Taking the functional derivative of Eq.17 and set it to zero, we obtain the following ordinary differential equation

$$\begin{aligned} \frac{\delta F[\theta]}{\delta \theta} &= \frac{\partial f}{\partial \theta} - \frac{\partial}{\partial \beta} \left(\frac{\partial f}{\partial \theta'} \right) \\ &= \frac{R + r \cos \beta}{r} \left(1 - \frac{r^2 \cos^2 \beta}{(R + r \cos \beta)^2} \right) \sin 2\theta \\ &\quad + 2 \sin \beta \theta' - 2 \frac{R + r \cos \beta}{r} \theta'' \\ &= 0 \end{aligned} \tag{18}$$

where f is the free energy density, and θ' and θ'' denote the first and second derivatives of θ with respect to β , respectively. There are two kinds of boundary conditions in this problem, the first one is

$$\theta(0) = \theta(2\pi), \theta'(0) = \theta'(2\pi) \tag{19}$$

and the second one is

$$\theta(0) = 0, \theta(2\pi) = \pi \tag{20}$$

.

With the first boundary condition, the solution of θ is symmetric with π , i.e. $\theta(\beta) = \theta(2\pi - \beta)$, from this symmetry the first derivative of θ has to be zero at $\beta = 0$ and $\beta = \pi$. With this condition, the boundary value problem (18) with boundary condition

$$\theta'(0) = \theta'(\pi) = 0 \tag{21}$$

can be solved by the shooting method. Starting from $\beta = \pi$ for a guessed $\theta(\pi)$ and $\theta'(\pi) = 0$, the equation can be integrated to $\beta = 0$ to obtain $\theta(0)$ and $\theta'(0)$, adjusting the $\theta(\pi)$ according

to the deviation of calculated $\theta'(0)$ from 0 and integrate it again till convergence. The calculated result for $k = 0.8$ is shown In Fig.2. In this case the calculated $\theta(\pi) = 1.369226$, $\theta(0) = 0.107654$ respectively.

Figure 2 is the variation with respect to β the θ and θ_β for $k = 0.8$. On the outer circle where $\beta = 0$ the θ is small so that the nematic vector is only slightly away from the symmetry circle, it is increased monotonically and reaches the maximum value at $\beta = \pi$, the inner circle. The maximum value is slightly smaller than $\pi/2$. This is typical for all k 's above a critical value k_c , below it a non-zero solution to the equation (18) with BC1 does not exist.

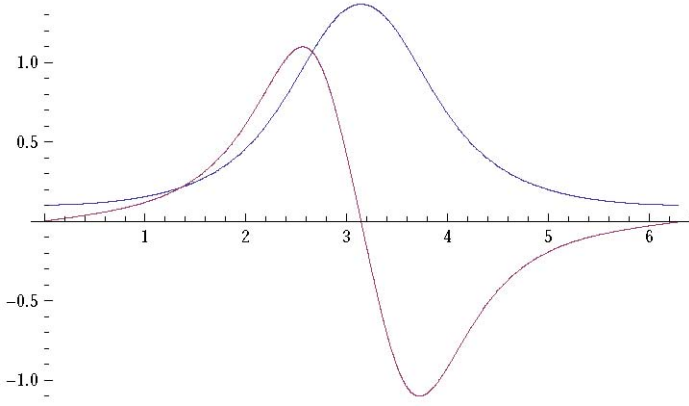


Figure 2. variation of θ (blue) and θ_β (red) with β as calculated from the solution of (18) for $k = 0.8$.

In order to determine the critical value k_c , we construct an eigenvalue problem with λ as the eigenvalue to be determined:

$$-\theta'' + \frac{\sin \beta}{(k^{-1} + \cos \beta)}\theta' + \frac{1}{2} \left(1 - \frac{\cos^2 \beta}{(k^{-1} + \cos \beta)^2} \right) \sin 2\theta = \lambda \theta \quad (22)$$

The spectrum of the λ is a continuum with a lower bound, the minimum eigenvalue λ_{\min} . If the minimum eigenvalue λ_{\min} is positive, the only solution for the original equation is the constant one and when λ_{\min} is negative it is clear that there is a non-constant solution. The minimum eigenvalue is a function of k , and when $k = k_c$ the minimum eigenvalue is zero. The minimum eigenvalue for different k can be calculated numerically by solving the eigenvalue equation (22), the result is shown in figure3. From the calculation the critical value of k is determined to be $k_c = 0.659$.

The non-zero solution for the case that k is slightly above k_c , $k = 0.66$, is given in figure 4. In this case, $\theta(\pi) = 0.1258247$ and $\theta(0) = 0.00965636$ respectively, which is very small and close to zero. Figure 5 gave the value $\theta(\pi)$ as a function of k in the vicinity of the critical point k_c . Below k_c , $\theta(\pi) \equiv 0$ and $\theta(\pi)$ increases monotonically above k_c . By a log-log curve fitting of the data above k_c , we found that the $\theta(\pi)$ follows a power law form close to k_c with the exponent 0.5, i.e. $\theta(\pi) \sim (k - k_c)^{0.5}$.

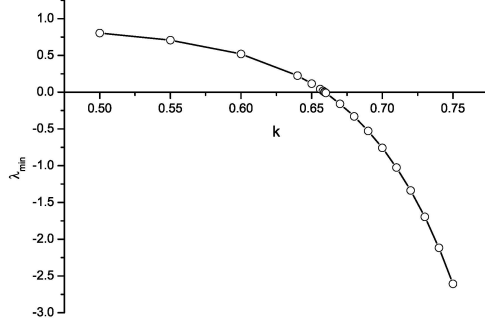


Figure 3. The minimum eigenvalue λ_{\min} as function of k .

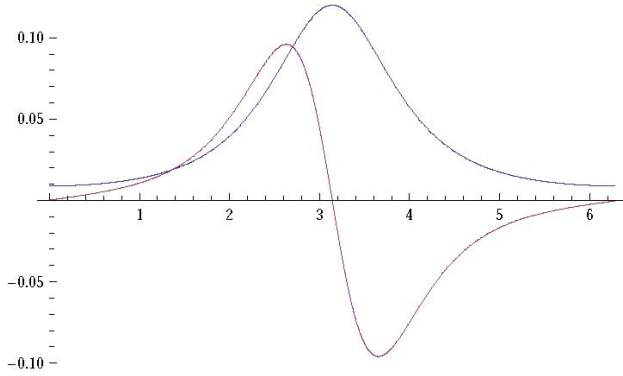


Figure 4. The non-zero solution of θ for $k = 0.66$, just above the $k_c = 0.659$. The blue line is the $\theta(\beta)$ and the red line is the $\theta'(\beta)$ respectively.

Next let us solve Eq.18 with the second boundary condition (BC2)

$$\theta(0) = 0, \theta(2\pi) = \pi \quad (23)$$

At $k = 0.8$, the solution is showed in Fig.6. Note that its mirror solution is solution of Eq.18 $\theta(0) = 0, \theta(2\pi) = -\pi$. It is clear the two chiral solutions have the same free energy. We

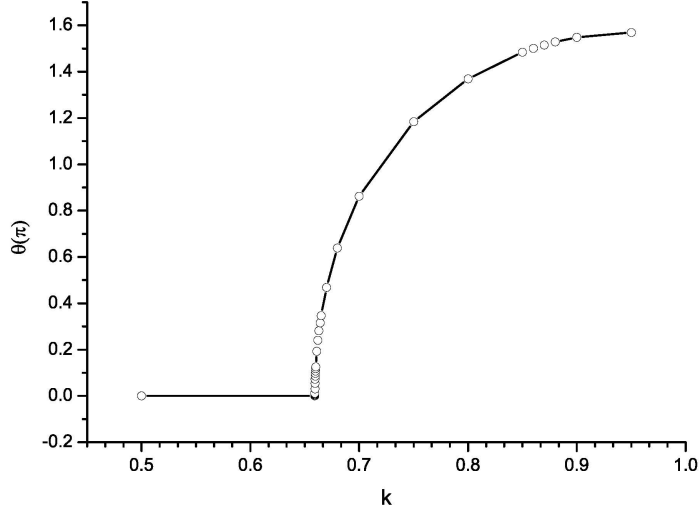


Figure 5. Variation of the $\theta(\pi)$ with respect to k in the vicinity of k_c

compare free energy of the solution under BC1 and BC2 in Fig.7. Free energy with BC1 always lower than the one with BC2. When k is large, the free energy difference becomes very small. When k is below k_c , zero-solution is the ground state and the free energy has an analytical form

$$F_k = \frac{4k\pi^2}{\sqrt{1-k^2}} \quad (24)$$

For the solution with BC2, the free energy gets its minimum at $k \simeq 0.72$. Although the solution with BC2 has larger free energy than the one with BC1, but it is topological stable if once formed unless thermal fluctuate is large enough to destroy it wholly and cross the free energy barrier.

Apart from the above analysis, we checked our results by the simulated annealing Monte Carlo calculation for the discrete free energy (4). In order to give a quantitative comparison, the total number of triangles of the surface mesh is around 4×10^4 . The initial temperature $k_b T/K$ is set to 1, then it is decreased by $T_{new} = T/1.0005$ every 10^3 Monte Carlo steps. The simulated defect-free state at $k = 0.8$ is shown in figure 8, from which we confirm the axis-symmetry condition is indeed true for this model. Figure 9 plots $\theta(\pi)$ in the vicinity of k_c , the line is from the solution of the Eulerian equation and symbols are from simulation, the quantitative agreement between the two are satisfactory.

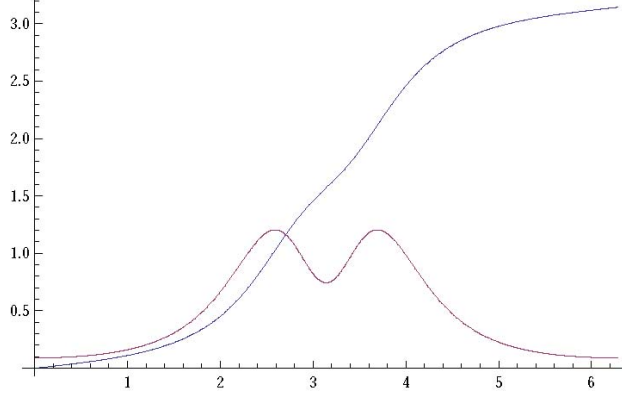


Figure 6. $k=0.8$. Blue Line: $\theta(\beta)$. Red Line: $\theta'(\beta)$. with $\theta(0) = 0, \theta(2\pi) = \pi$

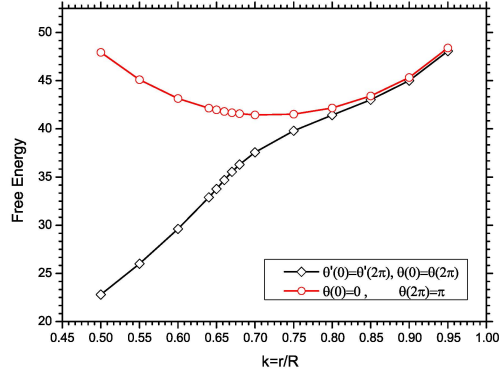


Figure 7. Free energy for 2 sets of boundary conditions

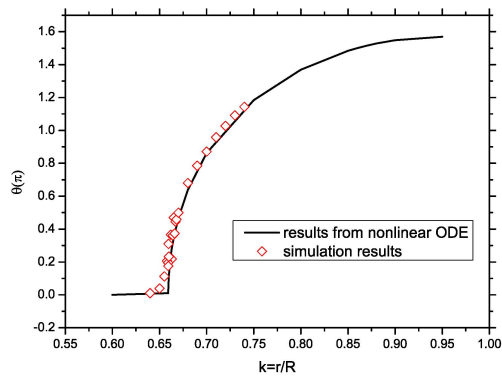


Figure 9. $\theta(\pi)$ of the ground state, compare of simulation and analytical results

Now we turn to the covariant gradient model (3), which can be rewritten as[?]]

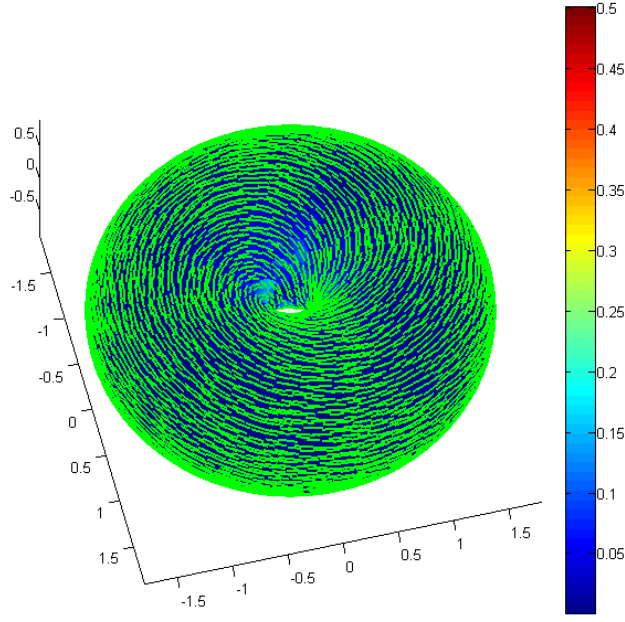


Figure 8. Simulation result of defect-free state at $k = 0.8$

$$F_{Frank} = \int [K (\nabla\theta + \mathbf{A})^2] dA \quad (25)$$

where $\mathbf{A} = (\hat{X}_\alpha \cdot \partial_\alpha \hat{X}_\beta, \hat{X}_\alpha \cdot \partial_\beta \hat{X}_\beta)$ is the spin connect. The analysis and discussion of the defect-free solutions of this model was given in Ref. [?] . The defect-free states are infinite continuum degeneracy configurations that θ equals to an arbitrary constant angle everywhere. We checked here the results by using simulated annealing Monte Carlo simulation with discrete model Eq.5. Our calculation indicates that the orientation angle θ is indeed a constant with random value which confirms the result in [?] . A representative state at $k = 0.8$ are shown in Fig.10. It is clear that the defect-free state of covariant gradient model is very different from 3D gradient model. To clarify this difference, we rewritten the 3D gradient model Eq.3 as [?]]

$$F_{Frank} = \int [K (\nabla\theta + \mathbf{A})^2 + K (\hat{n} \cdot \mathbf{K} \cdot \mathbf{K} \cdot \hat{n})] dA \quad (26)$$

where \mathbf{K} is the curvature tensor. Compared to Eq.25, Eq.26 has the additional term $\hat{n} \cdot \mathbf{K} \cdot \mathbf{K} \cdot \hat{n}$, which is the extrinsic coupling between nematic order and the curvature tensor, favoring aligning the nematic order along small curvature direction.

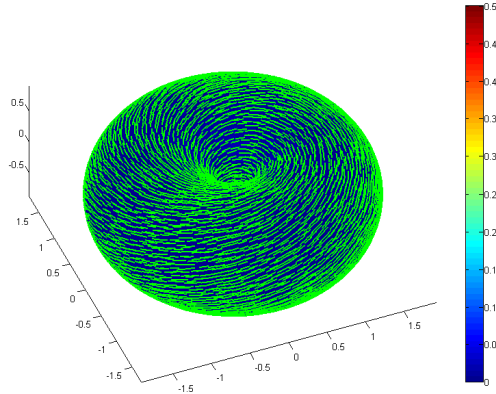


Figure 10. Defect-free state of covariant gradient model at $k = 0.8$

B. Topological defects

Now we turn to the more interesting case of topological defects. Defect-free states is the simplest case that the Poincaré-Hopf theorem can be satisfied, however states with topological order can also satisfy the Poincaré-Hopf theorem provided that the defects appear in pairs so that the total $\chi = 0$.

Headless nematic vector is a 2-atic order, which has the π rotational symmetry. Thus the winding numbers of least energetically expensive topological defects in nematic field are $\pm\frac{1}{2}$. When defects presents, the symmetry of rotation around z axis is no longer exist, thus the analysis through the Euler equation is much harder than the defect-free case. We do not attempt to perform such an analysis, instead, we use the simulated annealing Monte Carlo method to investigate. The computation load in the defect-free case and the case with topological defects is basically the same and the algorithm is reliable based on the simulation of the defect-free problem which gave the quantitative correct results.

Figure 11 shows a typical configuration with one pair of topological defects for $k = 0.8$. and Figure 12 shows its 2D projection to the $\alpha - \beta$ plane. As we can see that the $+1/2$ defect is located on the outer of the torus where the Gaussian curvature is positive, and the $-1/2$ defect is located at the inner of the torus where Gaussian curvature is the most negative. It is known that the topological defects on curved membrane behaviors in a way similar to an electrostatic problem. In this analogy the positive Gaussian curvature plays the rule of a negative charge distribution, and positive topological defect plays the rule of

a positive point charge[Nelson Review]. So the high positive Gaussian curvature geometry attracts positive topological defects, and vice versa. The pair of defects is in fact a direct result from simulation, i.e., when we starting the calculation from a random configuration and lower the temperature subsequently, both defect-free state or the state with defects may appear. The configuration of two pairs of defects are also observed, which is shown in Fig.13, and its $2D$ projection to $\alpha - \beta$ plane is shown in Fig. 14. The two $+1/2$ defects are located on the outer, and the two $-1/2$ defects located on the inner, as expected from the electrostatic analogy.

The ground state is the defect-free state and the state with topological defects are the excited states. When the positive and negative defects of a defect pair is close enough the two will annihilate, however, there is a potential barrier between the two defects which prevent the two close to each other. The barrier height determines the life time of the excited states. For fat torus the barrier height is high so that the life time of the states with defects is long, while for thin torus of smaller k , the barrier is low and the life time of the excited state is short. In the simulation calculations defects are not observed for thin torus.

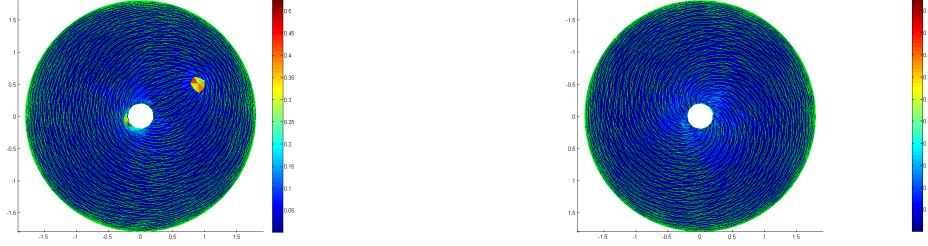


Figure 11. The configuration with a pair of defects for direct derivative model, top view(left) and bottom view (right)

For the covariant derivative model, a typical configuration with two pairs of defects is shown in figure 15, along with its $2D$ projection to $\alpha - \beta$ plane is shown in figure 16. Similar to the $3D$ direct derivative model, the two $+1/2$ defects are located on the outer part of the torus, and the two $-1/2$ defects are located on the inner part. A striking feature of this model compared to the previous one is that all the defects are located at the middle plane of the torus ($\beta = 0, \pi$). This is a result of the mirror symmetry about the middle plane of the orientation field. The second difference is that for a relative thin torus at $k = 0.6$, we also observed the configuration of two pairs of topological defects as shown in figure 17, while

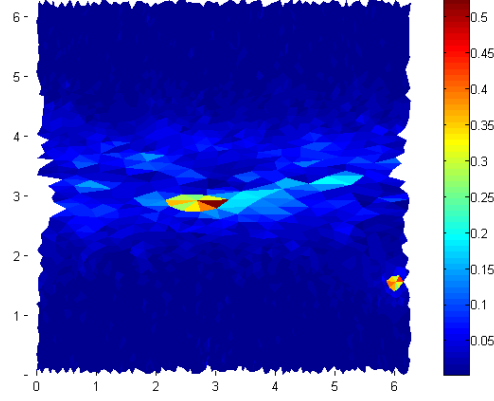


Figure 12. Projection to the $\alpha - \beta$ plane of the configuration in figure 11, the two defects are clearly seen.

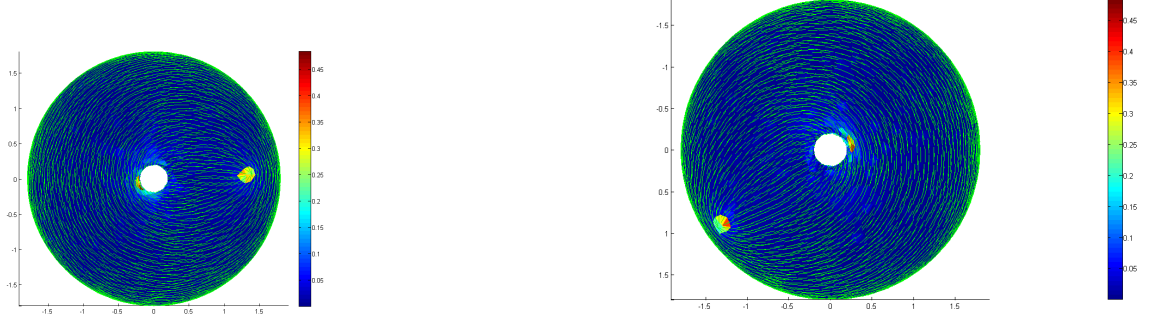


Figure 13. The configuration with two pairs of defects for direct derivative model

for a $3D$ direct derivative model no configuration with defects is observed at $k = 0.6$. This results are consistent with the theoretically predicted ground eigenstates 2_1 by Evans[?].

IV. CONCLUSION

In summary, we calculated the nematic ordering on a torus with both the standard and covariant Frank free energy models. We found that the ground state of the standard model is $\theta = 0$ for small k and θ varies with β for larger k . The transition point $k_c = 0.659$ is determined numerically from an eigenvalue problem. It is found that $\theta(\pi)$ changes continuously from 0 to non-zero at k_c in a power law form and the exponent was determined to be 0.5, i.e., $\theta(\pi) \sim (k - k_c)^{0.5}$ for k close to k_c . We also calculated the nematic configuration

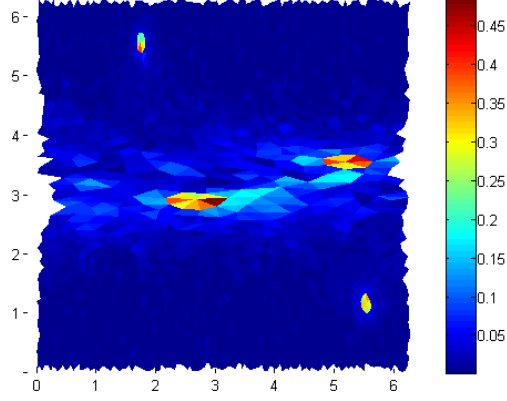


Figure 14. Projection to the $\alpha - \beta$ plane of the configuration in figure 13, the four defects are clearly seen in the figure.

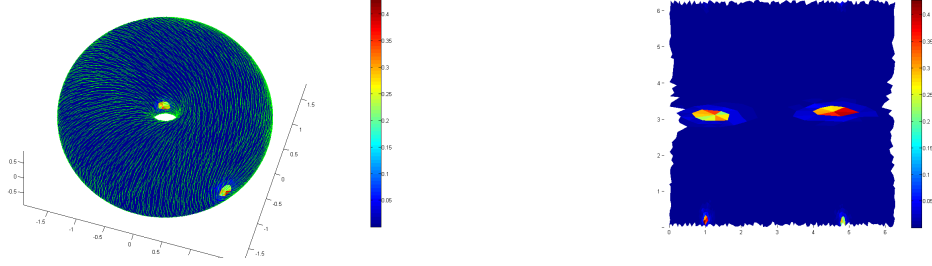


Figure 15. 2 pair of defects, $k=0.8$, direct dot Figure 16. 2 pair of defects, $k=0.8$, 2D projection

for k above k_c . All these results were obtained from the solution of the Eulerian equation of the free energy functional and checked by the Monte Carlo simulated annealing method. In the case of the covariant model, we confirmed the ground state is the θ equals to a random constant, which was proposed by Evans in Ref.?. The excited states are the states with pairs of defects. In the simulation, we observed one pair and two pairs defective states in both models. The positive defects are located on the outer part of the torus and the negative ones are on the inner part. The results can be understood by the analogy with an electrostatic problem where the Gauss curvature plays the rule of a continuous negative charge distribution. The excited state, when created, can stay for very long time because the barrier for the annihilation of a defect pair is fairly high for fat tori. This means that the defect state is experimentally observable and we hope that future experiment will reveal such state.

Work supported by the National Nature Science Foundation of China under grant

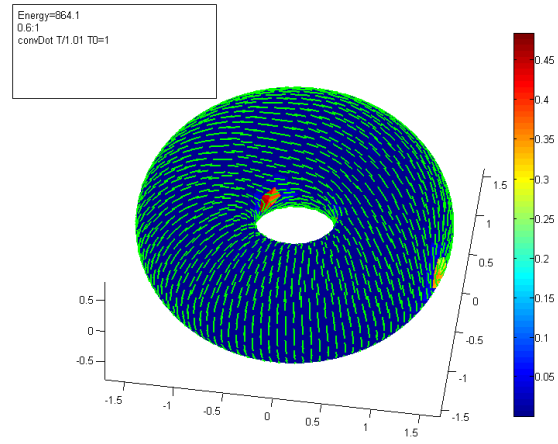


Figure 17. 2 pair of defects, $k=0.6$

#10874111, #11304169 and #11174196.